INSTITUTE OF PHYSICS PUBLISHING JOURNAL OF PHYSICS D: APPLIED PHYSICS

J. Phys. D: Appl. Phys. **34** (2001) A87–A92 www.iop.org/Journals/jd PII: S0022-3727(01)20269-1

Calculation of two-dimensional maps of diffuse scattering by a real crystal with microdefects and comparison of results obtained from three-crystal diffractometry

V P Klad'ko[1], L I Datsenko[1], J Bak-Misiuk[2], S I Olikhovskii[3], V F Machulin[1], I V Prokopenko[1], V B Molodkin[3] and Z V Maksimenko[1]

[1] Institute of Semiconductor Physics, National Academy of Sciences of Ukraine, Prospekt Nauki 45, 03028 Kyiv, Ukraine
[2] Institute of Physics, Polish Academy of Sciences, Al. Lotnikow 32/46, 02-668 Warsaw, Poland
[3] G.V. Kurdyumov Institute for Metal Physics, National Academy of Sciences of Ukraine, Vernadskogo blvd. 36, 03680, Kyiv 142, Ukraine

E-mail: kladko@isp.kiev.ua

Received 13 September 2000

Abstract
Two-dimensional maps of x-ray diffuse scattering (DS) in a reciprocal space for a real crystal containing Coulomb deformation centres (clusters or dislocation loops) were calculated using a new dynamical theory developed for a crystalline media with homogeneously distributed defects. Such maps were calculated for both the fundamental, 400, as well as the quasi-forbidden, 200, reflections of x-rays (CuKα_1 radiation) for a binary crystal (GaAs). They were also discovered experimentally in the GaAs films heavily doped with Si (up to 10^{20} cm^{-3}) by means of a Philips three-crystal diffractometer. The procedure for fitting calculated values of differential DS to the experimental data enabled not only the integral characteristics of the structure's perfection (Debye–Waller static factor, L_H, and coefficient of extinction of radiation due to additional energy losses on defects, μ_d) but also the average radius, $\bar{r}$, and concentration, $\bar{n}$, of microdefects (precipitates to be obtained).

1. Introduction

Diffuse scattering (DS) of x-rays is used nowadays to investigate structure defects in crystals [1–13] and DS theories have been developed and generalized by many authors [1, 5–7]. These studies have been dedicated to investigating defects in massive single crystals as well as in thin films and the surface layers of crystals [8, 9]. Double- as well as three-crystal spectrometers (DCS and TCS, respectively) have been used for experimental investigation of DS in such objects. These instruments are used in high-resolution diffractometry.

A TCS permits the intensity distribution in the reciprocal space near reciprocal lattice points (RELP) to be studied. A new informative and sensitive approach in three-crystal diffraction theory has recently been developed [14]. In this work important relations between the integral and differential intensities of the DS usually observed in the intensity profiles have been proposed. Such peaks are usually registered by the TCS at some angular deviations, $\Delta\theta$, of the sample under investigation from the exact Bragg position.

The aim of this paper was to investigate the real defect structure in GaAs films heavily doped with Si by analysing DS pictures registered by high-resolution diffractometry for both the usual and quasi-forbidden reflections (QFRs). It was also planned to calculate the isointensity contours of

© 2001 IOP Publishing Ltd Printed in the UK

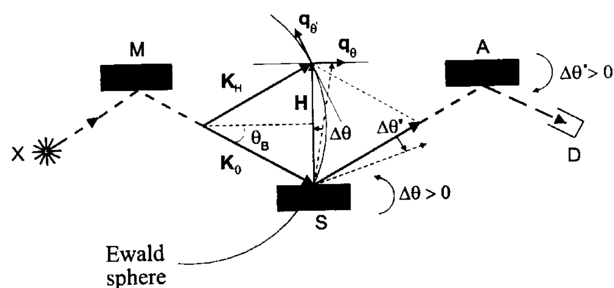

Figure 1. TCS scheme for measuring the intensity distribution of coherent as well as diffuse scattering in a reciprocal space. The notation: X, x-ray tube; M, monochromator; S, a crystal under investigation; D, detector. $\boldsymbol{K}_0$ and $\boldsymbol{K}_H$ are the wavevectors of the incident and diffracted waves respectively, $\boldsymbol{H}$ is the reciprocal lattice vector. $\Delta\theta$ and $\Delta\theta'$ are the angular deviations of the S and A crystals from their exact reflecting positions respectively. $\boldsymbol{q}_\theta$ and $\boldsymbol{q}_{\theta'}$ are the orths of the oblique coordinate system.

two-dimensional maps together with some of their sections using the previously mentioned theory [14].

2. Theoretical basis

Three-crystal spectrometry enables the diffuse component of the total reflectivity to be distinguished by analysing the character of the intensity distribution in a two-dimensional intensity map near the RELP [8, 9, 12, 13]. A scheme of a TCS is shown in figure 1. In our case the monochromator M was a Bartels-like unit set to obtain three-fold diffraction of the CuKα radiation. When the crystal S is turned through a small angle $\Delta\vartheta(\Delta\vartheta \ll \vartheta_B)$ the diffraction vector $\vec{H}$ rotates around the zero RELP. As a result of this movement the end of the wavevector of the diffracted beam, $\boldsymbol{K}_h$, is displaced along the axis q_ϑ, which is perpendicular to $\vec{H}$, for a distance $q_\vartheta = H\Delta\vartheta = 2K\sin\vartheta\Delta\vartheta$, $K = 2\pi/\lambda$. On the other hand, rotation of the crystal-analyser A through a small angle $\Delta\vartheta''(\Delta\vartheta' < \vartheta_B)$ enables the diffracted beams to be placed in various directions near the K_h direction. As a result of this second movement the working point of the TCS is displaced along the $q_{\vartheta'}$ axis which is perpendicular to K_h on the distance $K'_h\Delta\vartheta'$. So an oblique-angled system of coordinates exists. The angle between axes connected with diffraction planes in

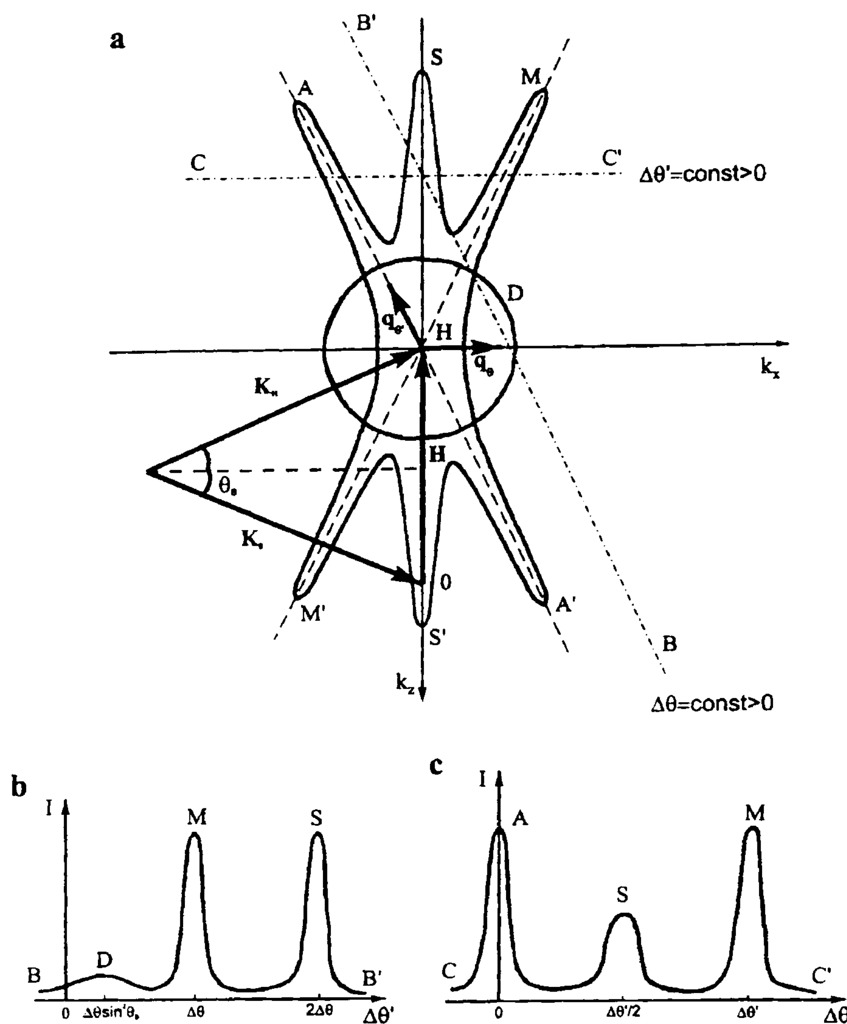

Figure 2. Characteristic shapes of isointensity contours for coherent (streaks A, M, S) and diffuse (circle) scattering measured by a TCS for symmetric Bragg diffraction (a) and an example of a TCS map measured by analyser scanning along the straight line BB′ ∥ $\boldsymbol{q}_{\theta'}$ at fixed $\Delta\theta$ (b) as well as by a sample S scanning along the straight line CC′ ∥ $\boldsymbol{q}_{\theta'}$ at fixed $\Delta\theta'$ (c).

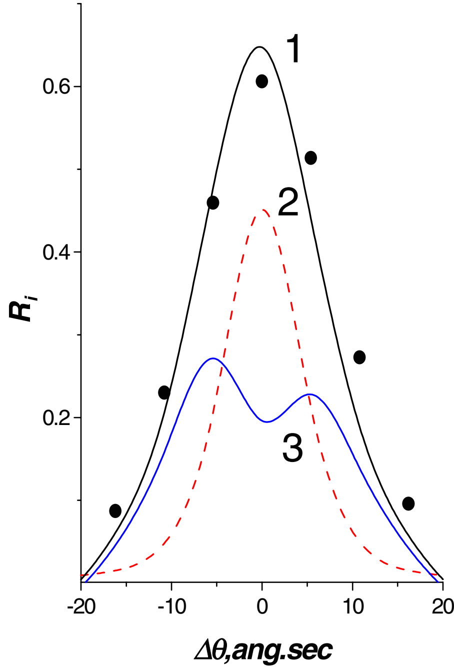

Figure 3. Experimental (points) and theoretical (full curves) diffraction rocking curves (CDR) for sample 1 obtained at $\Delta\theta' = 0$. All of the values are normalized by the intensity corresponding to the exact Bragg position. Curves 2 and 3 are the coherent (formula (3)) and diffuse (expression (4)) components respectively. 400 reflection of CuKα_1 radiation.

both crystals is equal to $\pi/2 + \vartheta_B$. Determining the angle coordinates of an analyser, $\Delta\vartheta'$, for a given level of DS intensity in the TCS map and, knowing the turning angle of sample $\Delta\theta$, one can determine the position of a working point in this set of coordinates. Marking the coordinates of various working points with a fixed DS intensity level one can plot the contours of equivalent intensity (isointensity lines) which enables the symmetry in defect deformation fields to be assessed [15]. One can also plot the isointensity contours for the coherent scattering by numerical treatment of the coherent intensity peaks (the so called 'resolution stars'). As a result of such procedures the isointensity contours for coherent (streaks) and diffuse (circle) (figure 2(a)) as well as the one-dimensional sections (figures 2(b) and (c)) can be obtained.

The total differentially scattered intensity R_S for monochromatic radiation for every position of a sample with homogeneously distributed Coulomb defects contains both a coherent, $R_B(q)$, and a diffuse, $R_{DS}(q)$, components [14]:

$$R_S(\vec{q}) = R_B(\vec{q}) + R_{DS}(\vec{q}) \tag{1}$$

where q is the distance from the nearest RELP.

Using the corresponding expressions for $R_B(q)$ and $R_{DS}(q)$ obtained in [14] for a real crystal and integrating them over the exit angles of a diffracted beam, one can determine the value of an intensity registered by the TCS. This intensity I_S depends on the angular variables, $\Delta\vartheta'$, $\Delta\vartheta$:

$$I_S(\Delta\vartheta, \Delta\theta') = I_B(\Delta\vartheta, \Delta\vartheta') + I_{DS}(\Delta\vartheta, \Delta\vartheta'). \tag{2}$$

The coherent I_B and diffuse I_{DS} components for every point of the isodiffuse map of the DS may be written for

Table 1. Structural characteristics (r_0, n_0) of precipitates in GaAs films dopped with Si as determined by the two independent methods.

Sample number	Fitting the theoretical CDR to experimental ones, 400 reflection	
	r_{01} (μm)	n_{01} (cm^{-3})
1	2.5	5.0×10^6
2	2.0	1.5×10^8

Note: the microdefect radii r_{02} also determined from intersection point q_0 of the $I_{DS}^{sym} = f(q)$ function with abscissa axis [16] are, respectively, 1.5 and 2.1 μm for samples 1 and 2.

the dispersion-free scheme of the TCS, i.e. $(n, -n, n)$ in the following way:

$$I_B(\Delta\vartheta, \Delta\vartheta') = I_0 \int \mathrm{d}x\, R_M\{b_M^{-1}[b_S^{-1}(x - \Delta\vartheta) - \Delta\vartheta]\} R_{coh}[b_S^{-1}(x - \Delta\vartheta)] R_A(x - \Delta\vartheta') \tag{3}$$

$$I_{DS}(\Delta\vartheta, \Delta\vartheta') = I_0 \int \mathrm{d}x\, R_M(x) \int \mathrm{d}x'\, r_{diff}(k_x, k_z) + R_A(x' - \Delta\vartheta'). \tag{4}$$

Here x is the angular coordinate of the deviation of the refracted beam from the exact Bragg position in a diffraction plane. Characteristics $R_M(q)$, $R_A(q)$, b_M and b_S stand for the reflection coefficients of the monochromator and analyser, the geometric parameters of asymmetry diffraction for a monochromator and specimen respectively. The function $r_{diff}(q_x, q_z)$ represents the differential diffuse component $R_{DS}(q)$ integrated over the region of vertical divergence, $\varphi = k_y/K$:

$$r_{diff}(q_x, q_z) = \frac{1}{K} \int \mathrm{d}q_y\, R_{DS}(q) \tag{5}$$

where K is the wavevector, $K = 2\pi/\lambda$, of the incident radiation with intensity I_0. The q_x and q_z components of the vector $\vec{q}$ are situated in the diffraction plane $(\vec{K}, \vec{H})$. At the same time these vectors are oriented, respectively, in the surface of sample, q_x, and perpendicular to it, q_z. They are given by

$$q_x = K(2\Delta\vartheta - \Delta\vartheta')\sin\vartheta_B$$
$$q_z = -K\cos\vartheta_B \Delta\vartheta'. \tag{6}$$

The profiles (section view scans) of the measured intensity distributions at a fixed position of a sample, $\Delta\theta_i$ = constant, as a function of the deviation of crystal-analyser $\Delta\theta'$ from the exact Bragg position, can also be obtained by means of a TCS. ϑ–2ϑ scanning in this unit enables the coherent component of reflectivity at the zero positions of the sample and analyser also to be analysed.

The expression for the coherent component of the reflection coefficient $R_{coh}(\Delta\vartheta)$ of a sample with a homogeneous distribution of defects [14], used to calculate the intensities (3), (4), has the following form:

$$R_{coh}(\Delta\vartheta) = \zeta(L - \sqrt{L^2 - 1}) \tag{7}$$
$$L = [z^2 + (g_0 + h)^2 + [(z^2 - (g_0 + h)^2 - E^2(1 - \kappa^2 - a^2)]^2] + 4(z(g_0 + h) - E^2(p_0 + d)]^{1/2}]/[E^2[(1 - \kappa_0^2 - a^2)^2 + 4(p_0 + d)^2]^{1/2}]^{-1}$$

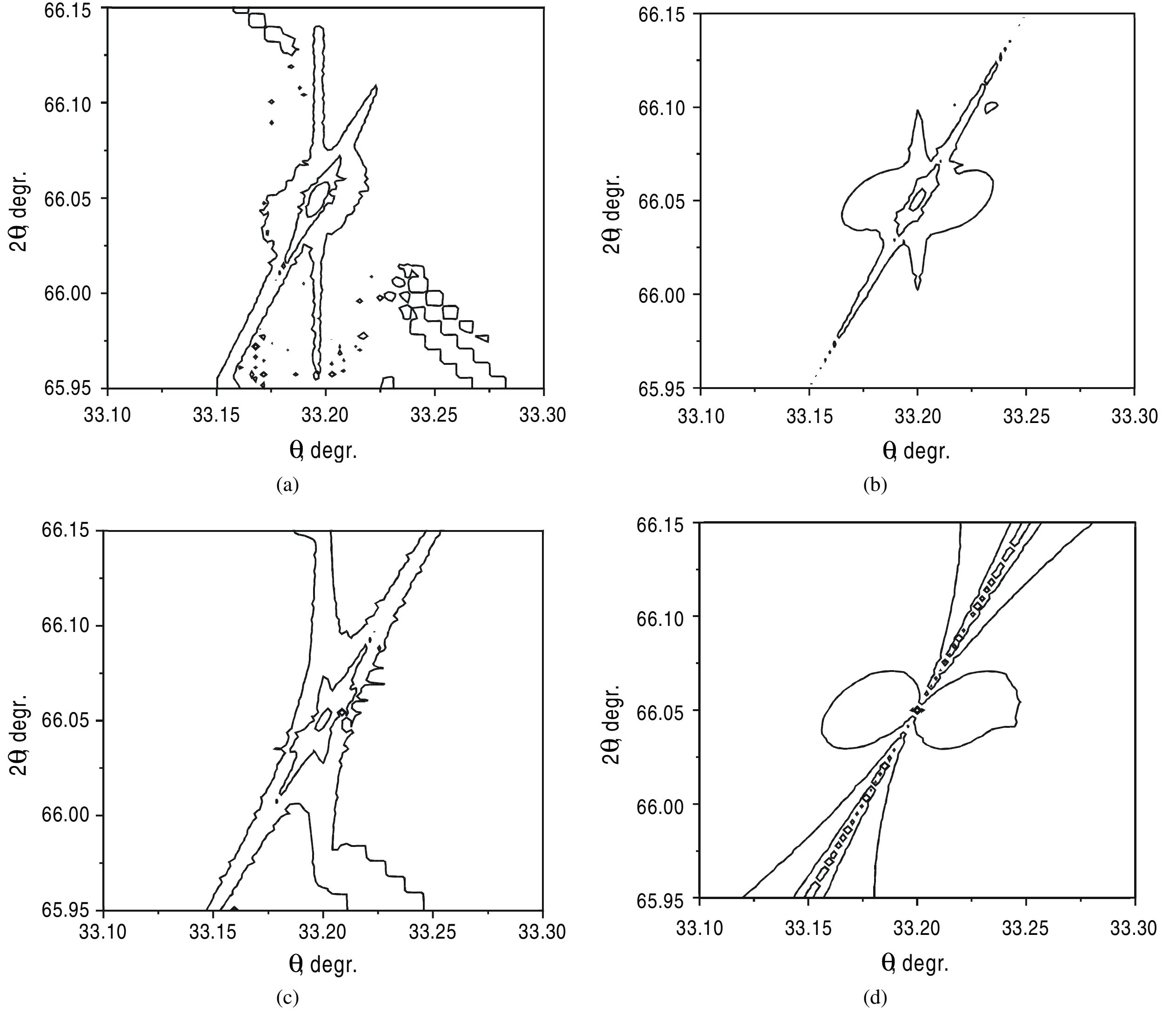

Figure 4. Experimental (a) and calculated (b) TCS maps (contours of lines of equal intensity) close to the 004 RELP for sample N2. Cu$K\alpha_1$ radiation. (c) and (d) correspond to the case of an almost perfect crystal ($n = 10^3$ cm^{-3}) and heavily distorted sample ($n = 10^9$ cm^{-3}). The radius of these defects is the same in all diagrams. The contour levels are 10 000, 5000, 100 and 5 counts s^{-1}.

$$z = \frac{\Delta\vartheta \sin^2\vartheta}{C \cdot \Psi_h}\sqrt{b}$$

$$\varsigma = |CE\chi_h + \Delta\chi^{\delta}_{h0}|/|CE\chi_{-h} + \Delta\chi^{\delta}_{0h}|.$$

Here, parameters g, κ and p are the same as in perfect crystal theory and take into account the absorption of coherent waves due to the inelastic scattering processes (photoelectric absorption, Compton effect, thermal diffuse scattering). The parameters h, d and a take into account the additional absorption of the coherent waves due to DS on defects, characterized by μ_{ds} and μ^*_{ds}. If the dispersion corrections to the Fourier coefficients of a susceptibility χ remain in the approximation for a semi-infinite crystal $\Delta\chi^{\delta}_{GG'} = P^{\delta}_{GG'} - \mathrm{i}\mu^{\delta}_{GG'}/K$ are denoted by

$$p_{GG'} = \mathrm{Re}\, P^{\delta}_{GG'}/(CE)$$

and

$$m_{GG'} = -\mathrm{Re}\, \mu^{\delta}_{GG'}/(KCE)$$

and the approximate equalities $p_{oh} \approx p_{h0}$ and $m_{0h} \approx m_{h0}$ hold, then these parameters can be represented by

$$h = (m_{hh} + m_{00}/b_S)\sqrt{b_S}/(2C|\chi_{rh}|) \qquad d = m_{h0}\chi'_{rh}/|\chi_{rh}|^2$$

$$\chi'_{rh} = \mathrm{Re}\,\chi_{rh} \qquad a^2 = (m^2_{hh} - p^2_{h0} - \chi'_{rh}p_{h0})/|\chi_{rh}|^2$$

$$E = \exp(-L_H).$$

The diffuse component of the reflection coefficient $R_{DS}(\Delta\vartheta)$ of a crystal with homogeneously distributed defects after integration over the output angles can be represented [14] as

$$R_D(\Delta\vartheta) = F_{din}(\Delta\vartheta)\frac{\mu_{ds}(k_0)\gamma_0}{2\mu_i(\Delta\vartheta)} \tag{8}$$

$$\mu_{ds}(k_0) = nC^2E^2m_0J_0(k_0) \qquad m_0 = \pi a^3(H|\Psi_h|/\lambda)^2/4$$

$$J_0(k_0) = b_2 \ln\frac{e(k^2_m + \mu^2_i)}{k^2_0 + \mu^2_i} + b_s\left(\frac{k^2_0}{2k^2_m} - 1\right)$$

$$\text{for } |k_0| \leqslant k_m$$

$$J_0(k_0) = \left(b_2 - \frac{1}{2}b_3\right)\frac{k_m^2}{k_0^2} \qquad \text{for } |k_0| \geqslant k_m. \tag{9}$$

Here H and n stand for the reciprocal lattice vector and the concentration of defects respectively; here, the defect radius e is the base of natural logarithm,

$$k_0 = K\Delta\vartheta\,\sin(2\vartheta) \qquad k_m = 2\pi/r_0$$

$$b_2 = B_1 + B_2\cos^2(\vartheta/2) \qquad b_3 = B_2\cos^2\vartheta(1 - 2tg^2\vartheta)/2.$$

For the spherical cluster model [16] the following expressions hold:

$$B_1 = 0 \qquad B_2 = (4\pi A_{cl}/a^3)^2$$

$$A_{cl} = \Gamma\varepsilon r_0^3 \qquad \Gamma = (1+\nu)/[3(1-\nu)]$$

ε is the deformation parameter and ν denotes the Poisson ratio.

3. Experimental details

The two-dimensional intensity distribution maps for GaAs films heavily doped with Si were measured by the three-crystal Philips diffractometer at the Institute of Physics PAS, Warsaw (figure 1). The $\Delta\vartheta$ profiles, i.e. the diffraction reflection curves, CDR, obtained without an analyser as well as the ϑ–2ϑ profiles for fixed positions of sample $\Delta\vartheta_i$, were taken for the 200, 400 and 600 reflections. The corresponding parameters for microdefects in the films under investigation (radius r_0 and concentration n_0) were determined by fitting the calculated reflectivities [15] to the experimental CDR as well as the maps of isointensity contours in a reciprocal space.

The Si concentration, n_{Si}, in the GaAs films was determined by means of second ion mass spectroscopy (SIMS) to be 2.5×10^{19} and 1.6×10^{20} cm^{-3} for samples 1 and 2 respectively. These values considerably exceeded the concentration p of charge carriers (holes) $p = 2$–5×10^{18} cm^{-3}. The difference between two values testified for large quantity of silicon atoms situated in an electrically passive interstitial positions. The thickness of samples 1 and 2 was rather large, i.e. 13 and 15 μm, which provided the possibility the reflectivities from the epitaxial films without taking into account scattering from the substrates to be registered.

4. Results and their discussion

Let us consider first the experimental results concerning the fundamental reflection 400 (points in figure 3) which shows the calculated rocking curve (CDR) 1 shown for sample 1. One can see relatively good agreement between the experimental and calculated CDRs obtained from formulas (1)–(9) of the dynamical theory of scattering by homogeneously distributed Coulomb deformation centres [14, 15]. One should stress here that these formulas also describe the behaviour of the DS component in the diffraction maximum region both for $r < \Lambda$ and $r > \Lambda$ (Λ is an extinction length distance).

The characteristics of microdefects in two GaAs:Si/GaAs films (r_{01} and n_{01}) determined by fitting the theoretical CDR curves to the experimental points are given in table 1. These happened to be close to those for $r_{02} = 1.5$ μm, obtained from the value of the scattering vector q_0 as determined from

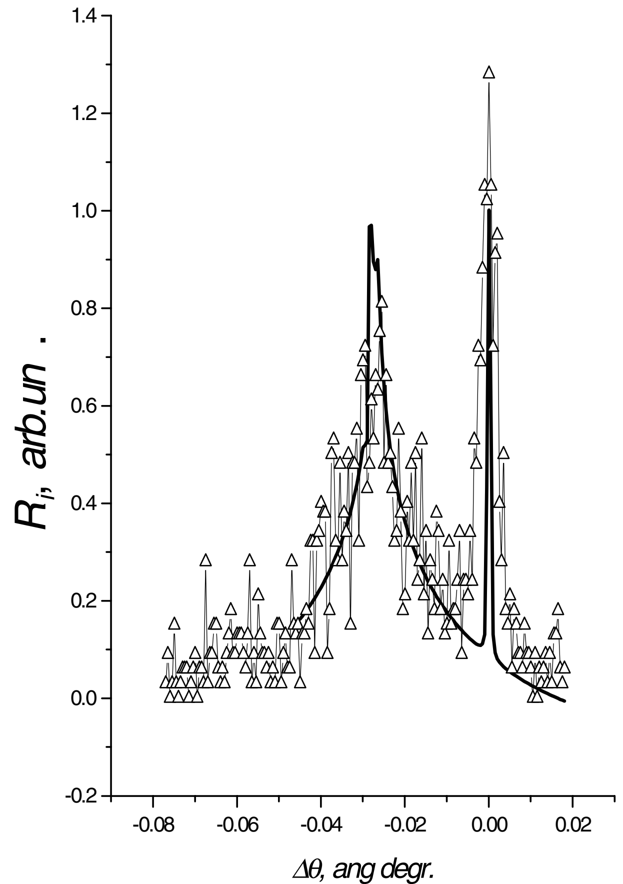

Figure 5. The experimental θ–2θ slice scan of the intensity distribution (triangles) as registered along the line parallel to the vector $\boldsymbol{H}_{400}$ taken at ($\Delta\vartheta = 0.030$) for sample 3. The result of this scan calculated for $r = 0.38$ μm and $n = 5.5 \times 10^9$ cm^{-2} is depicted by the solid curve.

the known method of the intersection point determination for the plot of $R_{DS} = f(\ln\Delta\vartheta)$ of the differential DS intensity with an abscissa axis [16]. Here R_{DS} and $\Delta\vartheta$, respectively, stand for the differential DS component of reflectivity and the angular deviation of the measured point from a RELP.

There was satisfactory agreement between all of the independent experimental values of radius r_0 and concentration n_0 of microdefects, obtained using the new analytical relations between the differential diffuse as well as coherent scattering components of the intensities, both integrated over the Ewald sphere [14, 15], and the characteristics of the microdefect structure testifies that the theory describes properly an x-ray interaction with the studied films.

One of the experimental isointensity maps of the two-dimensional distribution of the DS intensity registered near the 400 RELP together with previously mentioned 'resolution stars' due to the coherent part of the CuKα_1 scattering is shown for one of the films in the figure 4(a). The corresponding theoretical map (figure 4(b)) as calculated by formulas (1)–(9) is in qualitative agreement with the experimental ones (figure 4(a)). It was not possible to observe the characteristic minimum of the intensity distribution known for the case of spherical clusters due to the presence of the coherent scattering component. This minimum is only

seen in the calculated map (figure 4(d)) for the case of the heavily distorted crystal ($n = 10^9$ cm^{-3}) (kinematical limit of scattering). We have also calculated the intensity distribution for the almost perfect crystal ($n = 10^3$ cm^{-3}) shown in figure 4(c) in order to compare two limit cases (perfect as well as kinematical scattering crystal when the dynamical 'resolution star' is absent).

Quantitative agreement between experimental and theoretical data was shown in slice scans made from the experimental maps only. However, one can compare quantitatively different slice scans of a measured map. One such section taken along the line parallel to the diffraction vector $\boldsymbol{H}$ in the experimental map registered for another sample is shown in figure 5. The values of the radius $\overline{r}$ and concentration $\overline{n}$ of precipitates obtained by the fitting procedure for these two sections of the sample map are, respectively, 0.83 μm, 3.2×10^8 cm^{-3} and 0.38 μm, 5.5×10^9 cm^{-3}. The first group of parameters (larger radius and relatively lower concentration of defects) determines the level of the intensity registered more closely to the RELP 400. The second group of parameters describes the value of an intensity registered further away from the RELP.

5. Conclusion

Summarizing the results obtained in this paper one can note that the experimental as well as the calculated two-dimensional isointensity contours maps registered by the TCS in GaAs films heavily doped with silicon are in qualitative agreement. For different sections of the maps quantitative agreement was shown. Using a corresponding fitting procedure the parameters of the Coulomb deformation centres (precipitates) were also determined. Precipitates of various sizes and concentrations were shown to contribute to the intensities measured in different sections of the TCS maps.

The quantity of silicon atoms in GaAs (Si) films evaluated from values of the average radius and microdefect concentration is close in order of magnitude to that determined by SIMS.

References

[1] Kryvoglaz M A 1992 *Diffraction of X-ray and Thermal Neutrons in Imperfect Crystals* (Berlin: Springer) p 473

[2] Larson B C 1975 *J. Appl. Cryst.* **8** 150

[3] Mayer W, Grasse D and Peisl J 1985 *Phys. Status Solidi* a **87** 583

[4] Ehrhard P and Schilling W 1973 *Phys. Rev.* B **8** 2604

[5] Trinkaus H 1972 *Phys. Status Solidi* b **51** 307

[6] Trinkaus H 1972 *Phys. Status Solidi* b **54** 209

[7] Peisl H 1976 Structural information and defect energies studies by X-ray methods *Defects and Their Structure in Nonmetallic Solids* ed B Henderson and A E Hughes (New York: Plenum) p 381

[8] Kutt R N 1989 *Sov. Phys.–Solid State* **31** 270

[9] Kutt R N 1997 *Sov. Phys.–Solid State* **39** 1188

[10] Bonse U, Kappler E and Schill A 1964 *Z. Phys.* **178** 221

[11] Larson B C and Schmatz W 1974 *Phys. Rev.* B **10** 2307

[12] Eisenberger P, Alexandropoulos N G and Platzmann P M 1972 *Phys. Rev. Lett.* **28** 1519

[13] Ratnikov V V, Sorokin L M and Mosina G N 1981 *Sov. Phys.–Solid State* **23** 58

[14] Molodkin V B *et al* 2000 *Metal Phys. Adv. Technol.* **18** 1239

[15] Molodkin V B, Olikhovskii S I, Kislovskii E N, Krivitskii V P, Los' A V, Pervak E V, Ice G E and Larson B C 1999 *Metal Phys. Adv. Technol.* **17** 1383

[16] Dederichs P H 1971 *Phys. Rev.* B **4** 1041